Hindawi Publishing Corporation
Journal of Nanomaterials
Volume 2015, Article ID 198126, 6 pages
http://dx.doi.org/10.1155/2015/198126

Research Article

Graphene and Other 2D Material Components Dynamic Characterization and Nanofabrication at Atomic Scale

Wei Wang, Xing Wu, and Jian Zhang

Shanghai Key Laboratory of Multidimensional Information Processing, Department of Electrical Engineering, East China Normal University, 500 Dongchuan Road, Shanghai 200241, China

Correspondence should be addressed to Xing Wu; xwu@ee.ecnu.edu.cn

Received 18 October 2014; Accepted 30 December 2014

Academic Editor: Ching-Yuan Su

We demonstrate how abreaction corrected transmission electron microscopy (TEM) analysis techniques that are commonly used in nanostructure characterization can be used to study the morphology of graphene and other 2D materials at atomic scale, even subangstrom scale, and evolution of nanostructure and from which we determine the graphene components nanofabrication process. The key contributions of this work are perhaps focused on two areas: (1) recent progress on graphene characterization from the TEM aspect and (2) how the electron beam can be used to fabricate nanoribbon from graphene or similar 2D material.

1. Graphene Introduction

Graphene is made out of single-layer carbon atoms arranged on a hexagon structure [1] and is known for its outstanding material owning to its actual and potential applications [2]. It is a typical two-dimensional (2D) allotrope of carbon and hence has fascinating electrical, mechanical, and optical properties [3]. Due to the strong force between atoms in graphene, electron can hardly be interfered even when surrounding atoms are under crumpling in room temperature. The mobility of graphene can reach $2 \times 10^5\ \mathrm{cm^2V^{-1}s^{-1}}$, 140 times higher than silicon [4]. Its intrinsic strength is reported to exceed that of other crystalline structures, which provides potential value in the field of 2D composite material [5]. Theoretical and experimental results indicate that monolayer graphene can only absorb ~2.3% of incident white light and each layer adds another 2.3%, which means that the number of graphene layer can be estimated by its opacity [6].

Numerous efforts have been reported for the preparation of graphene with single or few layers, such as mechanical exfoliation of highly ordered pyrolytic graphite (HOPG) [7], chemical vapour deposition [8–11], and liquid phase exfoliation of graphite [12–14]. It is known that graphene is a zero gap material where the upper and lower bands are generated at the K point having a linear dispersion in the Brillouin zone (BZ) [15, 16]. If we introduce graphene nanoribbons (GNRs) narrowing the width of graphene into quasi-one-dimensional structures, band gap could be expended, which can be utilized as semiconductor for excellent switching speed and high carrier mobility for transistor operations [12]. It has been shown experimentally that zigzag and armchair GNRs edges result in different electronic properties. The zigzag edges appear to have a high density of electronic states at the Fermi level [17]. And the zigzag and armchair edges of graphene can be reconstructed and interconverted under transmission electron microscopy (TEM) [18]. Microscopic roughening is an essential reason for structural stability of 2D materials. The electronic, thermal, and mechanical properties of graphene are sensitive to the inevitable presence of defects [19] and grain boundaries [20]. Hence, it is quite important to get credible observation into atom structures. By using transmission electron microscopy (TEM), extensive wave structure has been found on single-layer graphene sheet with a magnitude of 1 nm [21].

2. TEM and EELS Introduction

TEM is a widely used technique for the physical characterization of semiconductor devices and thin films. TEMs are best known for imaging the morphology of a specimen, but a whole range of additional techniques is available in TEMs

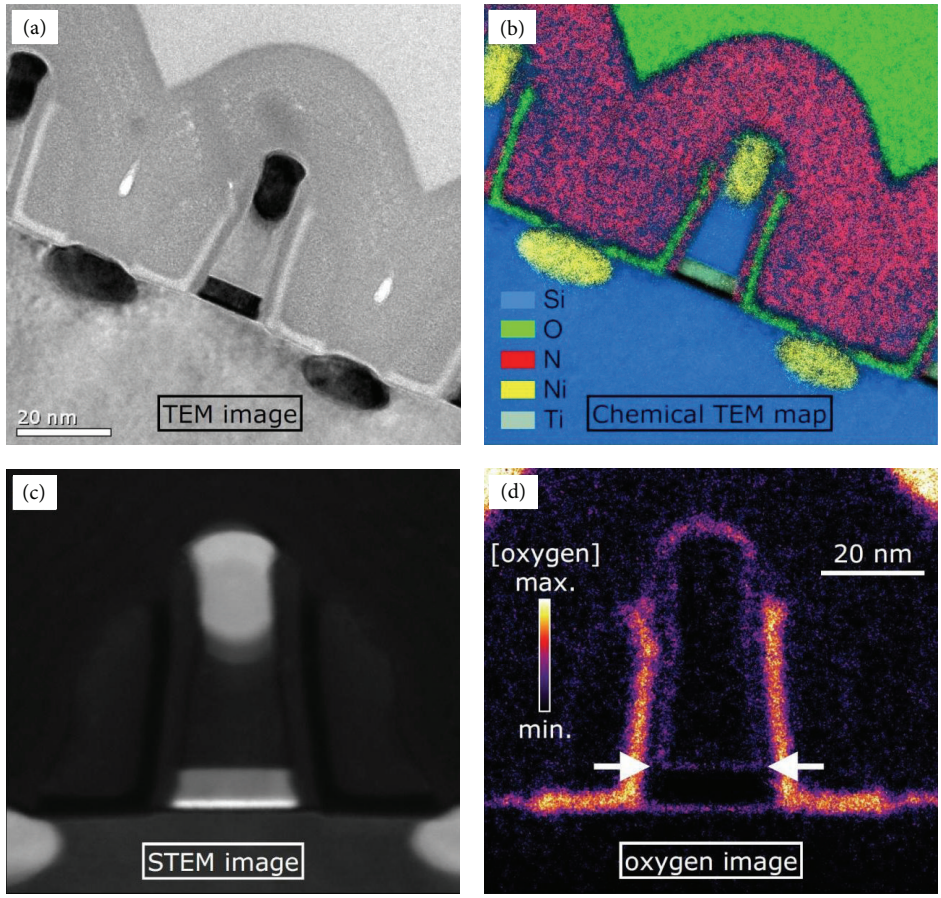

Figure 1: (a) Conventional TEM image of a MOSFET near the bottom in the silicon substrate, the source and drain and vertically in the center, the high-κ-containing gate stack. (b) Energy-filtered TEM image, with some of the chemical elements color-coded. (c) STEM ADF image of the same device, with the 3 nm thick high-κ layer showing bright. (d) Energy-filtered map similar to (b), but now showing the oxygen distribution in more detail. Spacers and gate oxide become clear, as well as a ~2 nm thick oxygen-containing layer between the gate metal and polycrystalline silicon.

to extract chemical, electrical, and structural information. By using the parallel electron beam of the TEM, for example, local diffraction patterns can be measured, which can provide accurate measurements of the crystal system and parameters. The electron beam could also be converged for diffraction measurements at even smaller areas of a few nanometers in diameter. Thus, the obtained converged beam electron diffraction pattern contains structural information in all three dimensions, as well as a means to accurately measure the specimen thickness.

A function often found on modern TEM is the STEM (scanning TEM) option. In this mode, the electron beam is further converged to a small probe with a diameter that can be varied from a few nanometers (for high-current measurements) down to the 0.1 nm (low-current) regime. STEM has only recently become a more widely used technique for the study of semiconductors. In the sections to follow, this paper will show the versatility of STEM for the study of semiconductor devices. In fact, it is often the only available characterization technique that can provide the necessary analysis of a device or interface. Its relatively recent growth in popularity in this field warrants a brief overview of STEM analysis.

STEM and TEM are usually performed with the same instrument; in fact, when a specimen can be imaged with TEM, it can also be imaged with STEM, likewise with atomic resolution. A comparison of STEM and TEM is given in Figure 1. In general, it can be said that TEM images reveal rich details on the morphology and crystal structure; STEM images often do not resolve polycrystalline structures. On the other hand, annular dark field (ADF) STEM images are much more directly interpretable. Their contrast reflects only two parameters: the (average local) atomic number and the specimen thickness. Therefore, if an area appears bright in an ADF STEM image, it is locally thicker or (more commonly) locally contains heavier elements. Figure 1(c), for example, immediately shows the presence of the hafnium-containing high-κ layer, which is much less obvious in the TEM image. Another advantage of STEM imaging is the lack of "TEM delocalization effects" at interfaces. Unless most spherical lens aberrations are corrected—which is only the case in high-end,

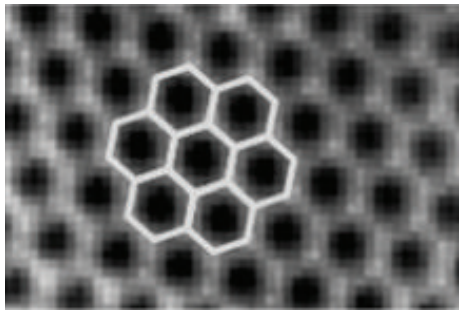

Figure 2: Hexagonal structure of monolayer graphene. Quoted from graphene sheets from worm-like exfoliated graphite [22].

corrected TEMs—the exact location of interfaces will often not be clear in TEM images. STEM images give more reliable information on the location and quality of an interface; they show directly where atom columns are located, in contrast to conventional TEM images.

Figure 2 shows the nanoscale structure of graphene. It shows direct morphology of honeycomb like structure. Figure 3 shows the evolution of graphene defects formation. Figure 4 shows the grain boundary of polycrystalline graphene. It is interesting to note that the grain boundary has no affection on the electrical transmission.

Both STEM and TEM can be used for chemical mapping, using electron energy-loss spectroscopy (EELS). In TEM mode, such an energy-filtered image is recorded for each element separately; for STEM, the whole EELS spectrum is recorded in parallel but acquired with only one image pixel at a time. Therefore, energy-filtered TEM maps are more efficient for imaging a large area, where many image pixels are needed. STEM on the other hand allows for a much more detailed spectral analysis of small areas or interfaces. Simultaneously with the acquisition of an ADF STEM image, EELS and EDX (energy-dispersive X-ray) spectra can be obtained. The combination of these techniques can give a comprehensive chemical analysis of a critical part of a device, with nanometer resolution. Due to the lateral nature of semiconductor devices, there is usually only one critical dimension for which nanometer-scale analysis is needed. An obvious example on which we will focus in this work is the chemical analysis of the various layers in gate stacks, for which line scans (or even point analysis) are usually sufficiently conclusive.

A few introductory words are in place regarding the analytical techniques EDX and EELS. When the small STEM probe travels through the specimen at a specific point, some of these fast electrons will interact with the specimen material. One interaction that will take place is the excitation of core-electrons. When this happens, some of the energy from the fast electron is transferred to the specimen electrons in the s, p, d, and so forth, core shells, which in turn are excited into empty energy states in the conduction band. Nearly immediately, a "free" or conduction electron will fill the empty core state, relieving the energy difference by emitting an X-ray. So, two effects occur: an X-ray is generated (this is detected with EDX) and the fast electron has lost some of its initial energy (this energy loss is detected with EELS). The peaks that are observed in EDX and EELS spectra are typical for each chemical element and core level and can therefore be used to chemically analyze the small area where the STEM probe is located. EDX spectra can be widely dispersed, covering all chemical elements. EELS has a much smaller energy dispersion, but higher spectral resolution. As a result, EELS can be used to study a few selected elements in much more detail. Not only the presence of these elements can be revealed, but also their bonding nature, since the shape of the EELS peak will be a reflection of the local density of unoccupied electron states. EELS can therefore in some cases be used to measure local changes in bonding type, shifts in the conduction band onset, and changes in valence states. Localized measurements of semiconductor band gap energies are also possible, but with a degraded spatial resolution of ~10 nm instead of less than 1 nm [1]. A word of caution is in place when accurate chemical profiles are required. For this, it is often recommended to use EDX instead of EELS. Due to the small, on-axis collection angle of EELS detectors, EELS maps or line scans are sensitive to changes in average atomic number [2]. As a rule of thumb: when the STEM image shows large contrast variations at the area of interest, it is recommended to use EDX and not EELS for chemical profiling. The following section will show examples of how to apply (S)TEM-EELS to the nanoscale characterization of advanced gate stacks.

3. Dynamic Fabrication of 2D Material

The 2D transition metal dichalcogenides have been studied for decades for their electronic, optical, and catalytic properties as well as specific mechanical properties [23], but how to shape them into nanoribbons has hardly been studied. Here we find a novel approach to fabricate uniform, robust semiconducting molybdenum sulfide ribbons with subnanometer width simply by *in situ* electron irradiation in a transmission electron microscope. It is shown that the sulphur atoms at the edge of a MoS_2 sheet are too fragile to stand against the electron beam, so that holes of defects, once being created, can rapidly spread and approach each other and form ribbons between them. When the ribbon width is narrowed to a critical size well below one nanometer, phase transition into a semiconducting Mo_5S_4 structure occurs spontaneously before the holes breaking into coalescence, which is mechanically strong and robust to the electron beam. This approach could be developed into a general controllable method for fabrication of subnanometer building blocks from transition metal dichalcogenide sheets for future functional devices.

Our *in situ* electron irradiation experiment starts with a monolayer MoS_2 sample prepared by micromechanical cleavage as identified by both optical (Figure 5(a)) and high resolution transmission electron microscope (HRTEM) characterization (Figures 5(b) and 5(c)). Under the irradiation of electron beam, defects can be created in the atomic thin 2D sheet once the beam energy exceeds the knock-on damage threshold of the sheet. The thresholds for removing sulphur and molybdenum atoms from a perfect MoS_2 sheet are calculated by first-principles theory to be 6.93 and 18.26 eV (Table 1 and [24]), respectively. Once a hole is created in the sheet, the

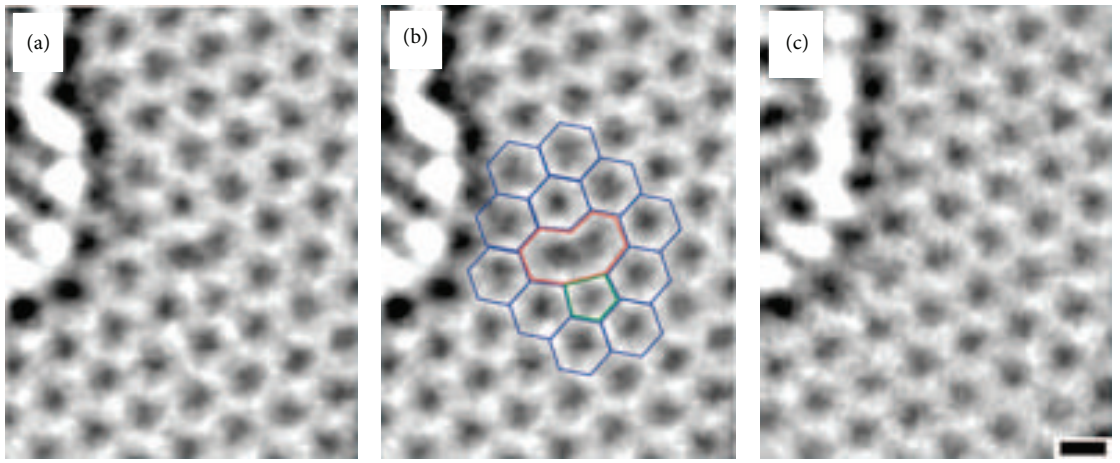

Figure 3: (a) HRTEM image of graphene. (b) Atomic configuration of (a). (c) Unperturbed lattice, few seconds later. Quoted from Direct Imaging of Lattice Atoms and Topological Defects in Graphene Membranes [19].

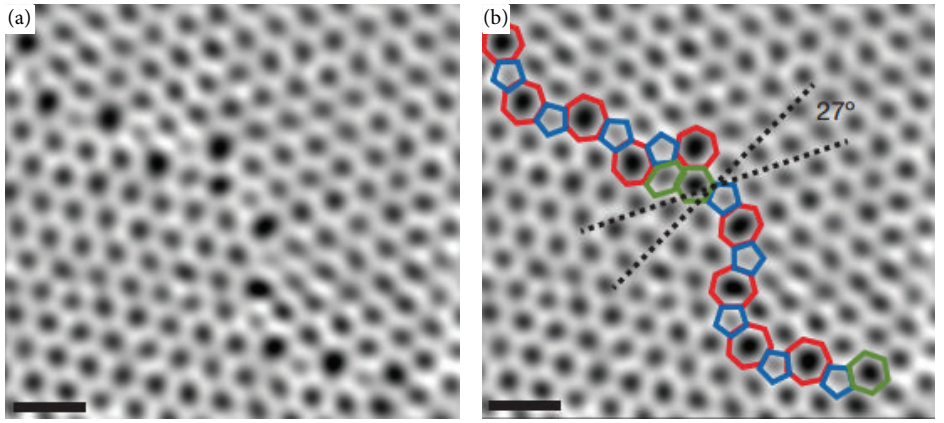

Figure 4: (a) Grain boundary of polycrystalline graphene. (b) Atomic configuration of (a), with hexagons (green), pentagon (blue), and heptagon (red). Quoted from Grains and grain boundaries in single-layer graphene [20].

Table 1: The nonrelaxed formation energies of chalcogen and metal vacancies E_f (eV)[‡].

	MoS_2		WS_2		$MoSe_2$	
	S	Mo	S	W	Se	Mo
MX_2 layer	6.1	13.9	6.3	15.3	5.6	12.4
Armchair ribbon[*†]	4.9	9.6	5.4	11.4	4.4	8.4
Zigzag ribbon[*†]	4.4	8.0	4.8	9.2	4.2	7.2
M_5X_4 ribbon[†]	6.8	8.8	7.1	9.8	6.0	8.7

[‡]The nonrelaxed E_f of chalcogen vacancy in monolayer MX_2 agrees with the displacement threshold [19].
[*]Armchair ribbon of five dimer lines and zigzag ribbon of four zigzag chains across width are considered.
[†]Edge chalcogen and metal vacancies in the armchair, zigzag, and M_5X_4 ribbons are chosen for formation energy calculations.

threshold for removing a sulphur atom from an armchair or zigzag edge is significantly reduced to 5.74 or 5.23 eV (Table 1), respectively. As the maximum energy transferred from an 80 kV electron to a sulphur atom is about 6 eV, between the thresholds of the edge and interior sulphur vacancies of the MoS_2 sheet, we chose an acceleration voltage of 80 kV to achieve enough resolution while maintaining the MoS_2 sheet in highly crystalline. The electron beam was firstly focused to 40 A/cm^2 to induce initial defects and holes in the MoS_2 sheet. After 81 seconds of irradiation, small vacancy aggregations formed as labelled by the arrows in Figure 1(d). As the edge of the defects is much weaker, all the defects spread rapidly in exposure to the irradiation. After another 103-second irradiation, the defects grew into holes with diameters of 3~6 nm as shown in Figure 5(e), with an average edge shrinking speed of about 0.02 nm/s. Along with the growth of holes, the connecting regions between them were narrowed into nanoribbons, showing a trend for coalescence. But just before the coalescence occurred, the thinnest connecting ribbon spontaneously turned into a fine ribbon with distinguished structural feature and uniform width of 0.35 nm (Figure 5(f)), which was robust to the dense electron irradiation. On the other hand, as the maximum transferred energy to Mo atoms is much less than the threshold for removing Mo atoms, aggregation of molybdenum at the edges of holes, especially at the ends of the fine ribbons, can be found.

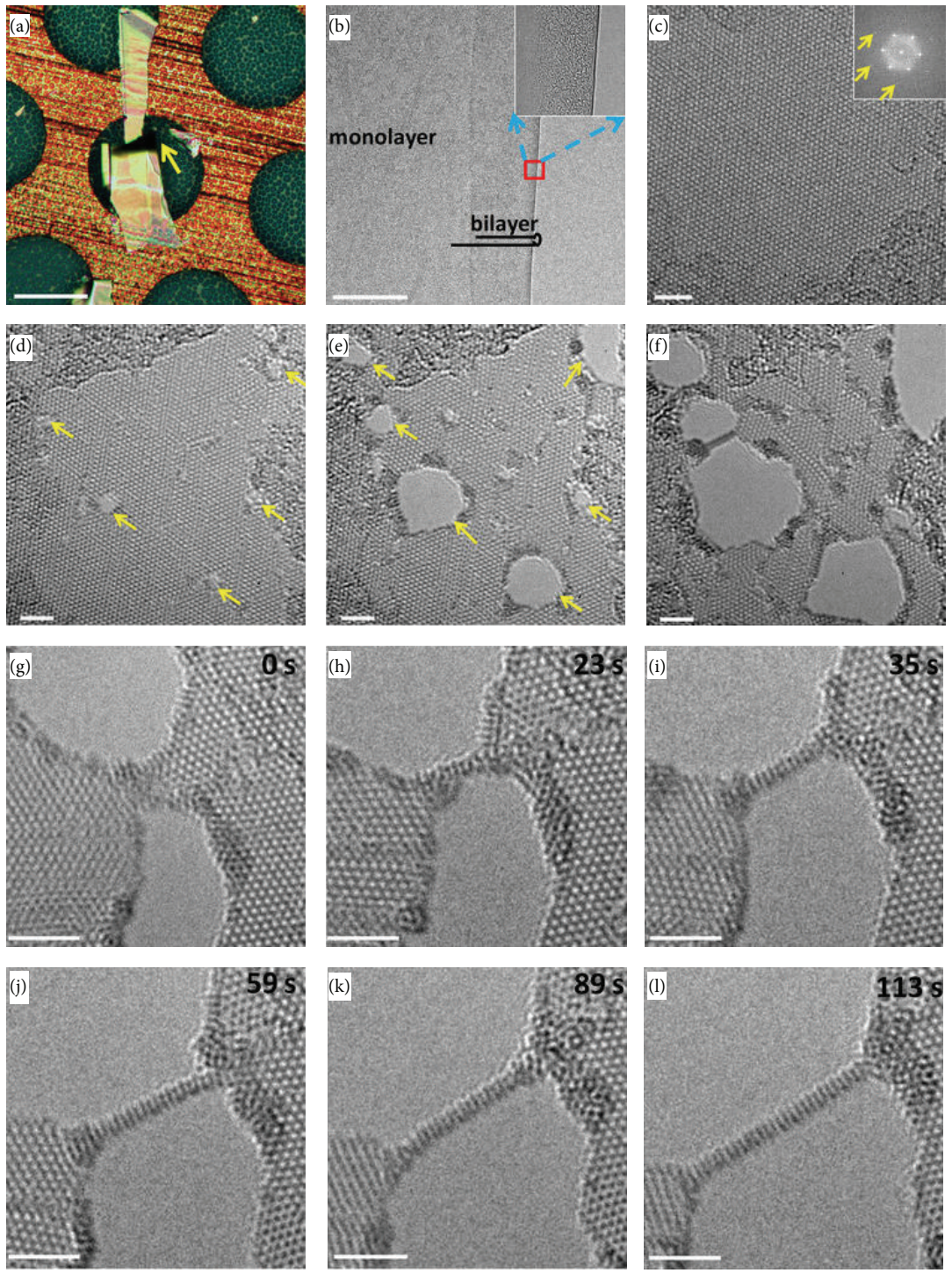

FIGURE 5: *In situ* fabrication of suspended molybdenum-sulfide subnanometer ribbons. (a) A few layer MoS_2 flake on transmission electron microscope (TEM) grid. The thinnest region locates at the region labeled by arrow. The scale bar is 100 μm. (b) TEM images of the thinnest region. The thickness of the membrane can be determined by fringe counting at the edge. The straight edge verifies that the membrane is single layer. The folded and unfolded region can be further determined by contrast. The scale bar is 100 nm. (c) High resolution TEM data obtained on the unfolded regions. The corresponding fast Fourier transformation (FFT) image is shown in the inset. (d) The initial MoS_2 membrane with small irradiation-induced vacancies as highlighted by the arrows. (e-f) Larger holes extended from the small vacancies upon 80 kV electron irradiation of another 108 and 261 seconds. (g–l) Time series of the formation and growth for a suspended subnanometer ribbon under 80 kV electron irradiation. The scale bars in (c–l) are 2 nm [24].

To carefully investigate the surprising fine ribbon, we decreased the beam intensity to 10 A/cm^2. The typical formation and elongation process for a fine ribbon was recorded in Figures 5(g) to 5(l). The formed ribbon showed uniform width with identical atomic structures, in sharp contrast to the mother MoS_2 at its ends.

4. Conclusion

We studied physical and chemical properties of graphene and introduced theoretical and practical use of TEM. Using TEM/EELS and STM techniques, we have successfully decoded the chemical nature of defects and grain boundaries of graphene. Then we developed a novel approach to fabricate uniform, robust semiconducting molybdenum sulfide ribbons with subnanometer width simply by *in situ* electron irradiation in a transmission electron microscope, and presented excellent experimental results.

Conflict of Interests

The authors declare that they have no conflict of interests.

Acknowledgment

This work is supported by the Research Grant East China Normal University.

References

[1] K. S. Novoselovet, A. K. Geim, S. V. Morozov et al., "Electric field effect in atomically thin carbon films," *Science*, vol. 306, no. 5696, pp. 666–669, 2004.

[2] K. S. Novoselovet, A. K. Geim, S. V. Morozov et al., "Two-dimensional gas of massless Dirac fermions in graphene," *Nature*, vol. 438, no. 7065, pp. 197–200, 2005.

[3] A. H. Castro Neto, F. Guinea, N. M. R. Peres, K. S. Novoselov, and A. K. Geim, "The electronic properties of graphene," *Reviews of Modern Physics*, vol. 81, article 109, 2009.

[4] K. I. Bolotin, K. J. Sikes, Z. Jiang et al., "Ultrahigh electron mobility in suspended graphene," *Solid State Communications*, vol. 146, no. 9-10, pp. 351–355, 2008.

[5] C. Lee, X. Wei, J. W. Kysar, and J. Hone, "Measurement of the elastic properties and intrinsic strength of monolayer graphene," *Science*, vol. 321, pp. 385–388, 2008.

[6] R. R. Nair, P. Blake, A. N. Grigorenko et al., "Fine structure constant defines visual transparency of graphene," *Science*, vol. 320, no. 5881, p. 1308, 2008.

[7] A. K. Geim and K. S. Novoselov, "The rise of graphene," *Nature Materials*, vol. 6, no. 3, pp. 183–191, 2007.

[8] A. Dato, V. Radmilovic, Z. Lee, J. Phillips, and M. Frenklach, "Substrate-free gas-phase synthesis of graphene sheets," *Nano Letters*, vol. 8, no. 7, pp. 2012–2016, 2008.

[9] A. Malesevic, R. Vitchev, K. Schouteden et al., "Synthesis of few-layer graphene via microwave plasma-enhanced chemical vapour deposition," *Nanotechnology*, vol. 19, no. 30, Article ID 305604, 2008.

[10] A. Reina, X. Jia, J. Ho et al., "Large area, few-layer graphene films on arbitrary substrates by chemical vapor deposition," *Nano Letters*, vol. 9, no. 1, pp. 30–35, 2009.

[11] K. S. Kim, Y. Zhao, H. Jang et al., "Large-scale pattern growth of graphene films for stretchable transparent electrodes," *Nature*, vol. 457, no. 7230, pp. 706–710, 2009.

[12] X. Li, X. Wang, L. Zhang, S. Lee, and H. Dai, "Chemically derived, ultrasmooth graphene nanoribbon semiconductors," *Science*, vol. 319, no. 5867, pp. 1229–1232, 2008.

[13] X. Li, G. Zhang, X. Bai et al., "Highly conducting graphene sheets and Langmuir-Blodgett films," *Nature Nanotechnology*, vol. 3, no. 9, pp. 538–542, 2008.

[14] Y. Hernandez, V. Nicolosi, M. Lotya et al., "High-yield production of graphene by liquid-phase exfoliation of graphite," *Nature Nanotechnology*, vol. 3, no. 9, pp. 563–568, 2008.

[15] M. Fujita, K. Wakabayashi, K. Nakada, and K. Kusakabe, "Peculiar localized state at zigzag graphite edge," *Journal of the Physical Society of Japan*, vol. 65, no. 7, pp. 1920–1923, 1996.

[16] K. Nakada, M. Fujita, G. Dresselhaus, and M. S. Dresselhaus, "Edge state in graphene ribbons: nanometer size effect and edge shape dependence," *Physical Review B—Condensed Matter and Materials Physics*, vol. 54, no. 24, Article ID 17954, 1996.

[17] J. Campos-Delgado, J. M. Romo-Herrera, X. Jia et al., "Bulk production of a new form of sp 2 carbon: crystalline graphene nanoribbons," *Nano Letters*, vol. 8, no. 9, pp. 2773–2778, 2008.

[18] Ç. Ö. Girit, J. C. Meyer, R. Erni et al., "Graphene at the edge: stability and dynamics," *Science*, vol. 323, pp. 1705–1709, 2009.

[19] J. C. Meyer, C. Kisielowski, R. Erni, M. D. Rossell, M. F. Crommie, and A. Zettl, "Direct imaging of lattice atoms and topological defects in graphene membranes," *Nano Letters*, vol. 8, no. 11, pp. 3582–3586, 2008.

[20] P. Y. Huang, C. S. Ruiz-Vargas, A. M. van der Zande et al., "Grains and grain boundaries in single-layer graphene atomic patchwork quilts," *Nature*, vol. 469, no. 7330, pp. 389–392, 2011.

[21] J. C. Meyer, A. K. Geim, M. I. Katsnelson, K. S. Novoselov, T. J. Booth, and S. Roth, "The structure of suspended graphene sheets," *Nature*, vol. 446, no. 7131, pp. 60–63, 2007.

[22] W. Gu, W. Zhang, X. Li et al., "Graphene sheets from worm-like exfoliated graphite," *Journal of Materials Chemistry*, vol. 19, no. 21, pp. 3367–3369, 2009.

[23] Y. Shi, W. Zhou, A.-Y. Lu et al., "van der waals epitaxy of mos2 layers using graphene as growth templates," *Nano Letters*, vol. 12, no. 6, pp. 2784–2791, 2012.

[24] X. Liu, T. Xu, X. Wu et al., "Top-down fabrication of sub-nanometre semiconducting nanoribbons derived from molybdenum disulfide sheets," *Nature Communications*, vol. 4, article 1776, 2013.